⌘ *Author's Choice*

THE JOURNAL OF BIOLOGICAL CHEMISTRY VOL. 286, NO. 46, pp. 39926–39932, November 18, 2011

Monitoring Single-channel Water Permeability in Polarized Cells*[S]

Received for publication, August 9, 2011, and in revised form, September 14, 2011 Published, JBC Papers in Press, September 22, 2011, DOI 10.1074/jbc.M111.291864

Liudmila Erokhova[‡], Andreas Horner[‡], Philipp Kügler[§], and Peter Pohl[‡1]

From the [‡]Institute of Biophysics, Johannes Kepler University and [§]Radon Institute for Computational and Applied Mathematics, Austrian Academy of Sciences, 4040 Linz, Austria

Background: The unitary permeability of water channels in polarized cells was immeasurable so far.
Results: We developed a new assay and validated it by determining aquaporin 5 water permeability in live epithelia on permeable support.
Conclusion: The assay accounts for both unstirred layer effects and changes in protein abundance because of trafficking.
Significance: New tool for investigation of water channel regulation/gating in signaling and drug development.

So far the determination of unitary permeability (p_f) of water channels that are expressed in polarized cells is subject to large errors because the opening of a single water channel does not noticeably increase the water permeability of a membrane patch above the background. That is, in contrast to the patch clamp technique, where the single ion channel conductance may be derived from a single experiment, two experiments separated in time and/or space are required to obtain the single-channel water permeability p_f as a function of the incremental water permeability ($P_{f,c}$) and the number (n) of water channels that contributed to $P_{f,c}$. Although the unitary conductance of ion channels is measured in the native environment of the channel, p_f is so far derived from reconstituted channels or channels expressed in oocytes. To determine the p_f of channels from live epithelial monolayers, we exploit the fact that osmotic volume flow alters the concentration of aqueous reporter dyes adjacent to the epithelia. We measure these changes by fluorescence correlation spectroscopy, which allows the calculation of both $P_{f,c}$ and osmolyte dilution within the unstirred layer. Shifting the focus of the laser from the aqueous solution to the apical and basolateral membranes allowed the FCS-based determination of n. Here we validate the new technique by determining the p_f of aquaporin 5 in Madin-Darby canine kidney cell monolayers. Because inhibition and subsequent activity rescue are monitored on the same sample, drug effects on exocytosis or endocytosis can be dissected from those on p_f.

Water channels may be gated by pH (1, 2), Ca^{2+} (3), phosphorylation (4, 5), mechanical stimuli (6), and voltage (7). Regulation of water channel activity also includes hormonally triggered exocytic channel insertion into the plasma membrane (8) and enzymatic control of endocytic retrieval (9). Ion channel research has revealed how difficult exploration of those processes is, although the sensitivity of available methods allows monitoring of single-ion channel activity. The lack of comparable methods renders the task even more difficult for AQPs.[2]

Available methods for acquiring the permeability (p_f) of single water channels are restricted to non-polarizable cells (oocytes) or model membranes. They are based on two experiments: measurement of the incremental permeability ($P_{f,c}$) introduced by the first ensemble of channels, and determining AQP copy number (n) in a second ensemble. In the ideal case, the ensembles are identical. But even if the very same sample could, for example, be subjected to electron microscopy after having survived the experiments for $P_{f,c}$ determination (10), and even if the time separation between the two measurements would be small, quantitatively assigning effects of posttranslational modifications or drugs to p_f or to n would be impossible. Analysis, for example by electron microscopy, simply destroys the sample. The long-debated effect of AQP2 phosphorylation on p_f illustrates the problem. The p_f increase remained hidden until purified AQP2 was reconstituted into proteoliposomes (5). The sole conclusion from cell experiments was that AQP2 phosphorylation increases n by triggering exocytic AQP2 insertion into the plasma membrane (8, 11).

Investigation of AQP regulation calls for polarized cells because they represent the native environment for most AQPs. Because their volume is a poor indicator of AQP-mediated water flux (12), measurement of the transepithelial water permeability, P_e, is the best choice. However, calculation of p_f requires dissection of the contributions of both channel-mediated apical membrane permeability ($P_{f,c}$) and basal membrane permeability (P_{bl}) to P_e.

Extended unstirred layers (USLs, stagnant water layers) represent another challenge. Their size increases with the size of the barrier; *i.e.* the USLs are large in the vicinity of an extended layer of cells that are all interconnected by tight junctions, adherens junctions, desmosomes, and gap junctions. As a consequence, transepithelial water flux may significantly dilute the osmolyte within the USL. The result is an overestimation of the

* This work was supported by Grants W1201 and P23466 from the Austrian Science Fund (FWF) (to P. P.).
⌘ *Author's Choice*—Final version full access.
[S] The on-line version of this article (available at http://www.jbc.org) contains supplemental Figs. 1–4, Table 1, and references.
[1] To whom correspondence should be addressed: Institute of Biophysics, Johannes Kepler University of Linz, Altenbergerstr. 69, 4040 Linz, Austria. Tel.: 43-732-2468-9269; Fax: 43-732-2468-9270; E-mail: peter.pohl@jku.at.

[2] The abbreviations used are: AQP, aquaporin; USL, unstirred layer; FCS, fluorescence correlation spectroscopy; MDCK, Madin-Darby canine kidney; PCMBS, *p*-chloromercuriphenylsulfonic acid.

actual driving force for water flow and the underestimation of epithelial water permeability (P_e) by a factor of two or more (13).

As we have shown previously, solute concentration measurements within the USLs solve the problem (14, 15). Instead of the previously exploited scanning ion-sensitive microelectrodes (14), we now use fluorescence correlation spectroscopy (FCS). From the rate of the dilution of an aqueous reporter dye in the narrow cleft between the cells and the cover glass, we correct for osmolyte dilution. For computational determination of P_e, we fitted a convection diffusion model to the measured non-stationary concentrations of the reporter dye (see "Experimental Procedures").

The main advantage of FCS as compared with scanning microelectrodes is that *n* of labeled AQPs becomes also attainable (Fig. 1). The data for both P_e and *n* are taken with negligible time delay, thus allowing the derivation of p_f. Because the sample is not destroyed, the procedure can be applied repetitively. To test the new approach, we used MDCK cells stably expressing AQPs.

EXPERIMENTAL PROCEDURES

Cell Culture—MDCK-C7 cells and stable cell lines overexpressing human aquaporin 1 (MDCK-hAQP1) and eYFP-tagged human aquaporin 5 (MDCK-hAQP5-enhanced YFP, kindly provided by V. Kolotovska, Upper Austria Research GmbH, Linz, Austria) were cultured in DMEM supplemented with non-essential amino acids, 5% fetal calf serum (v/v), 20 mM HEPES, penicillin, and streptomycin (all from PAA) at 37 °C in 7.5% CO_2. MDCK-AQP1 cells were kept under hygromycin B selection (75 μg/ml) and MDCK-hAQP5-eYFP cells under G418 selection (500 μg/ml). The cells (5×10^5) were either seeded onto polyester permeable supports (Transwell, Corning Life Sciences) or on glass slides. The Transwells were suited for transcellular water flow measurements. They had a surface area of 0.33 cm^2 and a pore size of 0.4 μm. Cell culturing continued until the formation of a tight monolayer (usually 4–5 days). We used the cells within 6 days after plating.

The cells on glass slides served for swelling experiments. We seeded about 2×10^5 cells per poly-L-lysine-covered 30-mm glass coverslip and used them within 3 days; *i.e.* before they reached confluence. All experiments were carried out in Hanks' balanced salt solution buffer at 37 °C.

Laser Scanning Microscopy and FCS—The heated stage of the confocal microscope (LSM 510, Carl Zeiss, Jena, Germany) carried the outer chamber (buffer volume 1.5 ml). Transwell inserts with cells (buffer volume inside 150 μl) were fixed on a micromanipulator and positioned at the center of the outer chamber at variable distances (z) to its glass bottom (80–140 μm) (Fig. 1).

Detection of reflection signals from both the insert membrane and the outer chamber glass bottom via a C-Apochromat water immersion objective (×40 magnification, numerical aperture = 1.2, Carl Zeiss) enabled precise measurements of z. The buffer in the outer chamber contained the fluorescent dye rhodamine B-labeled dextran MW 70000 (Sigma-Aldrich).

During the incubation time of about 15 min, we tested whether the MDCK monolayer allowed dye passage. Exclusion of rhodamine B from passage into the inner chamber served as an indicator for a tight monolayer. Subsequently, we established the transepithelial osmotic gradient by exchanging part of the insert buffer for the sorbitol-containing buffer or for distilled water. For aquaporin inhibition and for inhibition release, we added PCMBS (the mercury derivative *p*-chloromercuriphenylsulfonic acid, TRC, Inc.) and DTT (Sigma-Aldrich), respectively, to the apical side.

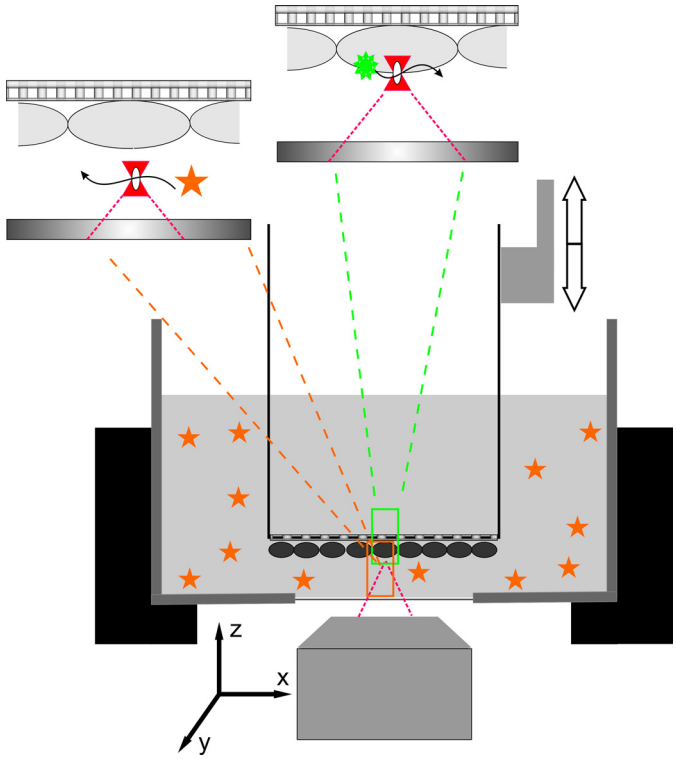

FIGURE 1. **Experimental setup.** A chamber with a glass bottom (thickness, 0.1 mm) was positioned into a thermo jacket on top of an inverse laser-scanning microscope (Zeiss, LSM510, Confocor 3). An additional micromanipulator positioned the MDCK monolayer, which was grown on the outer side of a Transwell filter at the desired distance from the glass bottom. Osmotic volume flow diluted the aqueous reporter dye (*orange stars*) when entering the outer compartment or increased its concentration when leaving the outer compartment. FCS measurements of reporter dye concentration (*left inset*, *orange rectangle*) enabled determination of epithelial water permeability, P_e. Supplemented by FCS measurements of YFP-aquaporin 5 density (σ) (*right inset*, *green rectangle*) abundance, the approach allowed the derivation of single-channel permeability (p_f).

Water flow into the cleft between the Transwell and the glass bottom of the chamber diluted the aqueous reporter dye. Water transport in the opposite direction increased its concentration because water dragged the dye from the bulk toward the epithelial barrier and because the dye was unable to follow the water through that barrier. To monitor these changes, we exploited a commercially available FCS extension to the LSM510 (Confocor 3, Carl Zeiss). FCS is based on the detection of small fluctuations in fluorescence intensity (16). Every entry of a labeled dextran molecule into the focal volume prompted an increase in fluorescence intensity (excitation at 561 nm; 15 milliwatt; 1% of maximal output; detection with a long-pass filter, 580 nm; pinhole size, 1 Airy unit). Measurement of the number of entries per unit time allowed calculation of dye concentration. The calculation algorithm included the computation of autocorrelation curves followed by applying the stan-

dard model for one-component free three-dimensional diffusion (17). The number of fluorescent particles in the detection volume (V_{eff}) was as follows,

$$N = V_{eff}C \quad \text{(Eq. 1)}$$

where C was the particle concentration. Repeating the 10-s measurement every 30 or 60 s enabled monitoring of dye concentration as a function of time.

We determined V_{eff} in the absence of the cell monolayer using tetramethylrhodamine (Sigma-Aldrich) as a reference dye. The diffusion coefficient of tetramethylrhodamine is equal to 4.5×10^{-6} cm^2/s (18).

The FCS technique also allowed estimation of hAQP5-eYFP abundance in the cell plasma membrane. We used the imaging facility of the microscope for positioning of the focus at the apical membrane of the desired cells. First we imaged their xy cross-sectional area. Then we performed a line scan in the z direction to determine the position of the apical membrane. After having shifted the focus to the intensity peak that corresponded to the apical membrane, we performed FCS. One FCS record consisted of six repeats of 40-s duration each. For fitting of the autocorrelation functions, we used the two-component equation for two-dimensional diffusion (19). The second (slow) component corresponded to the diffusion of the membrane protein. The excitation wavelength for cell imaging and FCS was 514 nm. The emitted light passed a 530–575-nm band pass filter. We calibrated the size of the confocal volume in the absence of cells using rhodamine 6G ($D = 4.26 \times 10^{-6}$ cm^2/s) (20).

Long-term focusing on one membrane spot causes photobleaching. Fluorescence intensity eventually reaches a steady state when the amount of bleached dyes per time interval is equal to the amount of dye molecules entering the focus from the surrounding area. As a consequence, FCS tends to underestimate N. To account for photobleaching, we calculated the ratio (r) of the initial and final fluorescence intensities, I_I and I_F, respectively. I_I was taken from the z profile (Fig. 5*b*), and I_F was set equal to the steady-state value of the FCS record. Multiplying N by r returned the real number of hAQP5-eYFP tetramers in the focal membrane area (A_F).

$$\frac{Nr}{A_F} = \frac{n_{ap}}{A_{ap}} = \frac{n_{bl}}{A_{bl}} = \sigma \quad \text{(Eq. 2)}$$

Our experiments revealed that the channel density (σ) was equal for the apical and basolateral membranes (with areas A_{ap} and A_{bl}, respectively).

Calculation of Epithelial Monolayer Permeabilities—To extract the osmotic water permeabilities P_{ce} and P_e of control monolayers and transfected monolayers, respectively, from the measured kinetics of dextran-rhodamine B concentration, we built a computational convection diffusion model and applied inverse problems techniques (for the full description, see supplemental material). The two-dimensional model is realized in COMSOL Multiphysics and takes into account the rotationally symmetric geometry of our experimental setup: the sizes of the insert (inner compartment), of the outer chamber (outer compartment), of the cleft between them, as well as the volume of the buffer (see supplemental Fig. 1).

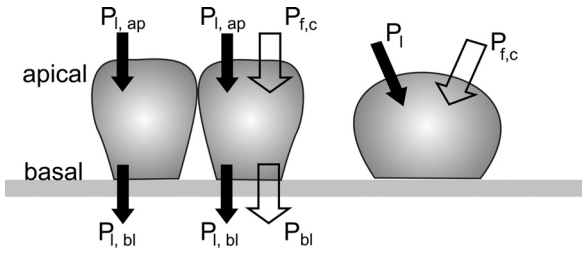

FIGURE 2. **Water pathways and permeabilities.** Water transport through MDCK monolayers is entirely transcellular. If no water channels are present (*left panel*), water transport is determined by the lipid permeabilities of the apical and basolateral membranes, $P_{l,ap}$ and $P_{l,bl}$, respectively. The incremental permeabilities, $P_{f,c}$ and P_{bl}, introduced by apical and basolateral channels facilitate water transport in cells transfected with aquaporins (*center panel*). Water entry into non-polarized MDCK cells leads to cell swelling. The swelling rate is determined by the lipid permeability P_l ($P_l = P_{l,bl}$) and the incremental permeability, $P_{f,c}$, which is introduced by the presence of aquaporins.

Calculation of p_f—The tight junctions of MDCK cells do not allow water flow (21). As a consequence, volume flow is entirely transcellular (Fig. 2). The apical and basolateral membranes behave like resistances in series, *i.e.* addition of their inverse permeabilities results in $1/P_{ce}$,

$$1/P_{ce} = 1/P_{l,ap} + 1/(F \times P_{l,bl}) \quad \text{(Eq. 3)}$$

where $P_{l,ap}$ and $P_{l,bl}$ are the permeabilities of the apical and basolateral lipids, respectively, and F is the ratio of the smooth basolateral membrane area (A_{bl}) to the smooth apical membrane area (A_{ap}) (7.63 in MDCK strain I (22)). Differences in glycosphingolipids and phospholipids contents (23) render $P_{l,ap} > P_{l,bl}$. Because the basolateral membrane and the membrane of non-polarized cells have the same lipid composition (24), we measured the permeability P_l of non-transfected, non-polarized cells (see below) and assumed that P_l is equal to $P_{l,bl}$.

Transfection of the cells with aquaporins alters both apical and basolateral water permeabilities. Denoting the combined water permeability of all apical and all basolateral aquaporins as $P_{f,c}$ and P_{bl}, respectively, and substituting P_{ce} for P_e transforms Equation 3 into Equation 4.

$$\frac{1}{P_e} = \frac{1}{P_{l,ap} + P_{f,c}} + \frac{1}{(P_{l,bl}+P_{bl})F} \quad \text{(Eq. 4)}$$

Assuming that the p_f values of aquaporins in the apical and basolateral membranes are similar, Equation 4 can be rewritten as follows.

$$\frac{1}{P_e} = \frac{1}{P_{l,ap} + \sigma p_f} + \frac{1}{(P_{l,bl} + \sigma p_f)F} \quad \text{(Eq. 5)}$$

σ is measured by FCS. P_e and $P_{l,ap}$ (via P_{ce}, Equation 3) are derived from the measured kinetics of dextran-rhodamine B concentration changes. Thus, Equation 5 enables calculation of p_f if $P_{l,bl}$ is obtained from experiments with non-polarized cells.

Experiments with Non-polarized Cells—We derived $P_{l,bl}$ from swelling kinetics of single untransfected cells grown on glass coverslips at 37 °C. First, we diluted the standard bathing solution (Hanks' balanced salt solution, 300 mOsm) with distilled water to establish an osmotic gradient of 150 mOsm and

recorded time series of cell x-z vertical sections in the reflection mode of the confocal laser scanning microscope. Fitting the time-dependent increase of the cell area with an exponential function returned the time constant τ. It allows calculation of P_l (25, 26),

$$P_l = \left(\tau\left(\frac{A_0}{V_0}\right)V_W C_{osm}\right)^{-1} \quad \text{(Eq. 6)}$$

where A_0, V_0, and V_W are the initial cell surface area, the initial cell volume, and the molar volume of water, respectively. In the case of non-transfected cells, we assumed $P_l = P_{l,bl}$.

To have an internal control for p_f, we repeated the swelling experiment with AQP5-eYFP-transfected cells. Calculation according to Equation 6 now revealed the combined lipid and channel permeabilities ($P_{l,c}$). The incremental permeability because of the presence of channels was then as follows.

$$P_{f,c} = P_{l,c} - P_l \quad \text{(Eq. 7)}$$

In addition, we measured the number, *n*, of YFP-AQP5 copies by the same procedure that we previously applied to polarized cells. Taken together, these experiments allowed calculation of p_f from swelling of non-polarized cells.

$$p_f = P_{f,c}A_0/n \quad \text{(Eq. 8)}$$

RESULTS

We first used the computational model to generate dye concentration profiles for different values of P_e *in silico* (Fig. 3*a*). For $P_e = 5$ μm/s (120-μm cleft thickness, 100-mOsm gradient, 40 min of volume flow), the model predicts that the dye concentration does not perceptibly depend on the space coordinate parallel to the membrane if measured within an interval of ± 1 mm from the center of the insert (*x* axis). In the same interval, the dye concentration varies by about 5% for $P_e = 25$ μm/s (supplemental Fig. 2). We also observed that a scan in the z direction is not required. The measurement of dye concentration at a single point at the center of the insert (in the xy plane) provides sufficient information. Restraining the measurements to a single point is beneficial as otherwise step motor movement causes vibrations, which in turn result in uncontrollable convection.

Fig. 3*b* shows the time profile of dextran-rhodamine B concentration for different osmotic gradients. In response to the increase in volume flow, the dye dilution becomes more pronounced. Reversing the sign of the gradient converts the dye dilution into an increase of dye concentration. Dye dilution also depends on the width (*w*) of the cleft between the cell layer and the bottom of the outer chamber. Averaging the outcome of all experiments led to P_e equal to (19 ± 2) μm/s (mean ± S.E.). Although measured at the same distance from cells, dye concentration changes faster for smaller *w* (supplemental Fig. 3). That is, minimizing *w* allows the detection of smaller water fluxes.

To demonstrate that the method is suited to monitor alterations of P_e that are induced by drugs, we blocked aquaporin 1 with PCMBS. It covalently modifies cysteine 189 and occludes the pore. The 4-fold decrease of P_e was reversed by DTT, which

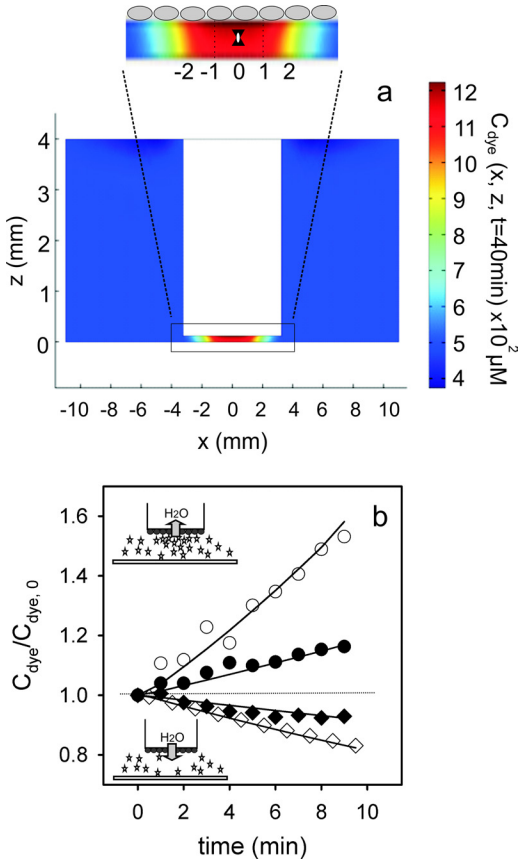

FIGURE 3. *a*, model simulation of the reporter dye (dextran-rhodamine B) concentration C_{dye} distribution. Water flows from the outer compartment through the epithelial monolayer into the Transwell insert. It drags the dissolved reporter dye to the epithelial barrier. Unlike water, the dye cannot pass through the monolayer. Consequently, its concentration in the epithelial vicinity increases. The snapshot depicts the theoretical C_{dye} distribution after 40 min of water flow. *x* and *z* denote the distances from center of the Transwell in the directions parallel and perpendicular to the cell monolayer, respectively. An enlarged view of the cleft between the Transwell and glass bottom is given in the *inset*. P_e and C_{osm} ($C_{osm} = C_{osm,\,ap} - C_{osm,\,bl}$) were 25 μm/s and +100 mOsm, respectively. Initial C_{dye} ($C_{dye,0}$) was equal to 50 nM. The model calculations were tested by FCS measurements of dye concentration. Therefore, the laser beam was focused on a position at some distance (z) from the middle (x = 0) of the Transwell. The cells were grown on the outside of the Transwell (see *inset*). *b*, C_{dye} reports P_{ce}. The experimental ratio $C_{dye}/C_{dye,0}$ was measured at the distance z = 60 μm from the MDCK-hAQP1 cell layer (x = 0). It is sensitive to C_{osm}: +350 mOsm (○), +100 mOsm (●), −100 mOsm (◇) and −50 mOsm (◆). + denotes sorbitol additions to the Transwell insert; − indicates dilution of aqueous solution within the Transwell by distilled water. The corresponding directions of water flux are given in the two *insets*. The *black lines* are theoretical fits to the experimental data. The only fit parameter, P_{ce}, was equal to (19 ± 2) μm/s.

recovers sulfhydryl groups to the reduced state (Fig. 4*a*). The P_{ce} of approximately 4 μm/s of non-transfected MDCK-C7 cells did neither respond to PCMBS nor to DTT (Fig. 4*b*). The P_e and P_{ce} values of both transfected and non-transfected MDCK cells agree well with results from scanning microelectrode measurements (27).

For the calculation of the single-channel permeability p_f of hAQP5-eYFP, we measured channel abundance in the plasma membrane. First, we took a confocal image of the cells grown on the permeable support (Fig. 5*a*). Then we recorded a z profile of eYFP-fluorescence of a particular cell (Fig. 5*b*). The fluorescence peaks corresponded to the apical (−5 μm) and basal (4 μm) membranes. Finally, we focused on the point correspond-

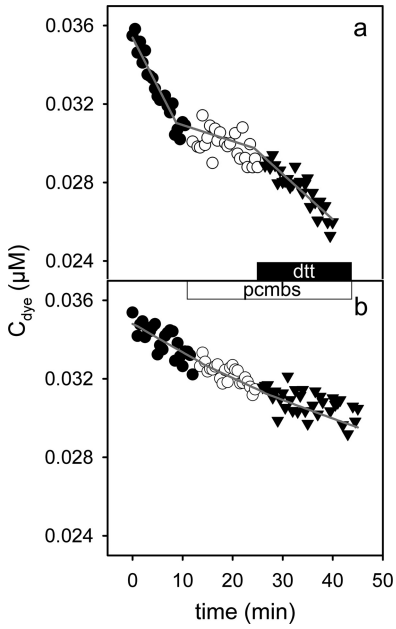

FIGURE 4. **Inhibition and release experiments.** C_{dye} was measured at z = 60 μm (x = y = 0) from MDCK-hAQP1 (*a*) or control MDCK-C7 (*b*) cell layers. The *dark gray lines* are outputs of the computational model fitted to the experimental data. The time intervals before addition of 0.6 mM PCMBS (●), between the additions of PCMBS and 5 mM DTT (○), and after DTT addition (▼) were fitted separately. *a*, the respective P_e values were approximately 18, 5, and 10 μm/s. *b*, P_{ce} was equal to 4–5 μm/s throughout the experiment. The cleft between cells and cover glass was 120 μm wide, and C_{osm} was −100 mOsm in both *a* and *b*.

ing to the apical membrane peak. From the autocorrelation curve at that position (Fig. 5*c*), we calculated the hAQP5-eYFP density σ. The repetition of the procedure for at least five cells returned an σ of approximately 232 ± 5.5 (mean ± S.E.) per μm^2. Identical fluorescence intensities in the z scan (Fig. 5*b*) indicate that σ is the same for both the apical and basolateral membranes.

Swelling experiments of non-transfected cells (supplemental Fig. 4) revealed $P_l = P_{l,bl} = 5.4 \pm 0.3$ μm/s. According to Equation 3, $P_{l,ap}$ is then equal to 4.4 ± 0.3 μm/s. In turn, Equation 5 indicates that p_f per individually diffusing particle is equal to $(6.3 \pm 0.5) \times 10^{-14}$ cm^3/s. Varying and even reversing the osmotic gradient gave the same result (Fig. 6). Taking into account the tetrameric structure of AQP5, the permeability of a monomer ($p_{f,m}$) is then equal to $(1.6 \pm 0.5) \times 10^{-14}$ cm^3/s.

DISCUSSION

We have shown that the *in vitro* determination of the monomer permeability $p_{f,m}$ from transcellular flux measurements is feasible in a single experiment. That is, we derived both *n* and $P_{f,c}$ from the same probe and with negligible time delay. An important advantage of the new FCS-based assay is that it allows $p_{f,m}$ investigation in polarized cells. It also allows monitoring of osmolyte dilution within the USL, precluding thereby the underestimation of $p_{f,m}$ (Fig. 2*d*).

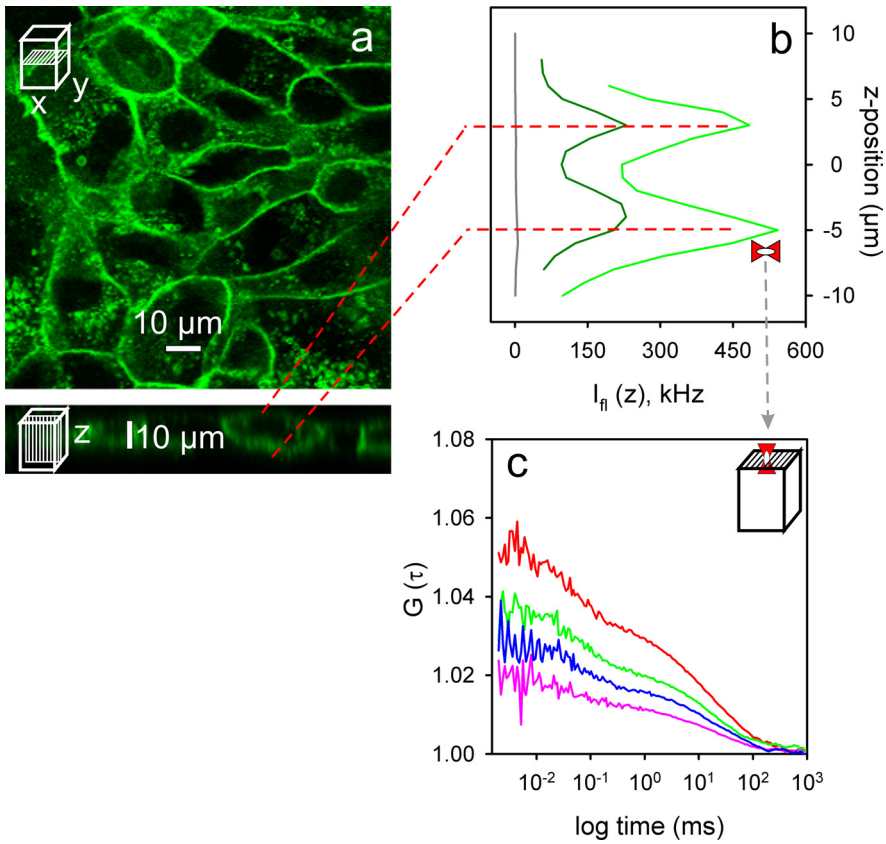

FIGURE 5. **Determining channel number N during osmotic challenge.** *a*, confocal image of AQP5-eYFP expressing MDCK cells on a Transwell insert. *Top panel*, xy section; *bottom panel*, xz-section. *b*, similar expression levels of AQP5-eYFP in the apical and basolateral membranes. The *graph* shows representative YFP fluorescence intensity z profiles of three different cells. The two intensity peaks belong to the apical and basolateral membranes. The *left gray line* shows background fluorescence. *c*, representative autocorrelation curves of AQP5-eYFP in the apical membrane of different cells from different monolayers. Differences in the amplitudes indicate different AQP5 densities: 30, 50, 60, and 90 tetramers (starting from the *upper curve*) per detection volume.

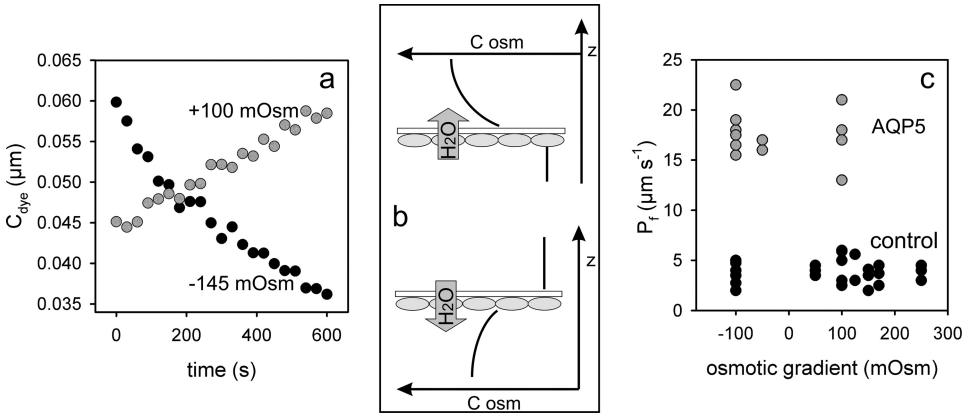

FIGURE 6. **Osmolyte dilution is taken into account.** *a*, water flow was directed either into the Transwell (+100 mOsm because of the presence of sorbitol, *gray circles*) or out of the Transwell (−145 mOsm because of the dilution of the internal buffer by water, ●). C_{dye} was measured at z = 60 µm (x = y = 0) from the MDCK-hAQP5-eYFP cell layers as a function of time that elapsed after establishing the osmotic gradient. *b*, schematic representation of osmolyte dilution. Because osmolytes with different diffusion coefficients (sorbitol *versus* NaCl) have been used and because different sizes of the osmotic gradient were applied, the level of osmolyte dilution in the epithelial vicinity must be different. *c*, nevertheless, P_e did not depend on the direction of the osmotic gradient. This result also indicates that the new assay properly accounts for the individual resistances of the apical and basolateral membranes. Cleft size was equal to 120 µm.

Our $p_{f,m}$ value is in reasonable agreement with a $p_{f,m}$ of approximately $(5 \pm 0.4) \times 10^{-14}$ cm^3/s obtained by oocyte swelling (28). In these experiments, the level of aquaporin 5 expression was normalized to the one of aquaporin 1 by recording autoradiograms of the immunoprecipitated proteins from microdissected oocyte plasma membranes. Therefore, [^{35}S]methionine was present in the incubation solution of the oocytes. Multiplication of normalized oocyte $P_{f,c}$ by $p_{f,m}$ of aquaporin 1 resulted in $p_{f,m}$ of aquaporin 5. Previously, the stopped-flow experiments with proteoliposomes and protein content determination from SDS-PAGE served to calculate a $p_{f,m}$ of approximately 6.8×10^{-14} cm^3/s of aquaporin 1 (29). The very same approach delivered a 2-fold larger aquaporin 1 $p_{f,m}$ of approximately 11.7×10^{-14} cm^3/s in the hands of other scientists (30). Freeze-fracture electron microscopy allows the derivation of $p_{f,m}$ without reference to experiments with reconstituted proteins. From the ratio of oocyte $P_{f,c}$ and particle density, the functional permeability of aquaporin 1 was estimated to be a $p_{f,m}$ of approximately 1.4×10^{-14} cm^3/s (10). If this value would have been taken as a reference, the calculations (28) would have revealed a 4-fold smaller $p_{f,m}$ for AQP5.

In contrast to immunoprecipitation or freeze fracture electron microscopy, our new assay works with live cells. It has the advantage that after having determined channel abundance, drugs or signaling molecules may still be administered, and their effect on channel abundance or $p_{f,m}$ may still be monitored. Moreover, any changes in P_e can be assigned unambiguously to $p_{f,m}$ or *n*. This feature should allow the dissection of drug effects on channel endocytosis or exocytosis from those on channel activity.

To further validate the new approach, we compared it to the traditional swelling assay. Fluorescence correlation spectroscopy still served to determine *n*. $p_{f,m}$ of approximately $(4.2 \pm 0.8) \times 10^{-14}$ cm^3/s from non-polarized cells on a glass plate that was in line with the $p_{f,m}$ from transepithelial flux measurements.

The comparison between flux values derived from swelling experiments and solute dilution just outside the monolayer should be done with caution because cell volume changes and transcellular water fluxes are essentially decoupled from each other (31). For example, vasopressin-induced cell swelling of inner medullary collecting duct cells depends on basolateral solute uptake via the Na-K-2Cl cotransporter and changes in actin organization via myosin II but does not depend specifically on increased apical water entry (31). A large vasopressin-induced transepithelial water flow in the absorptive direction may be detected without increasing cell volume (12). For example, epithelial monolayers were placed into a narrow tunnel so that upon osmotic challenge, the cross-sectional area of the current conducting buffer solution on top of these monolayers becomes smaller (32). Using the decreased electrical conductance as readout for an increased cell volume is straightforward. However, the link to aquaporin activity is less obvious. We therefore conclude that for the purpose of p_f determination, direct measurement of transepithelial water flow is mandatory.

In summary, the FCS-based assay enables investigation of water channel regulation/gating both by intrinsic cellular mechanisms and pharmaceutical drugs. It overcomes the limitations usually imposed by the presence of stagnant water layers (unstirred layers) adjacent to the epithelia because it accounts for osmolyte dilution. The new method paves the way for $p_{f,m}$ measurements of channels and transporters that are susceptible to their local environment, *e.g.* the presence of ordered domains or rafts.

REFERENCES

1. Yasui, M., Hazama, A., Kwon, T. H., Nielsen, S., Guggino, W. B., and Agre, P. (1999) *Nature* **402,** 184–187
2. Tournaire-Roux, C., Sutka, M., Javot, H., Gout, E., Gerbeau, P., Luu, D. T., Bligny, R., and Maurel, C. (2003) *Nature* **425,** 393–397
3. Németh-Cahalan, K. L., and Hall, J. E. (2000) *J. Biol. Chem.* **275,** 6777–6782
4. Törnroth-Horsefield, S., Wang, Y., Hedfalk, K., Johanson, U., Karlsson, M., Tajkhorshid, E., Neutze, R., and Kjellbom, P. (2006) *Nature* **439,** 688–694
5. Eto, K., Noda, Y., Horikawa, S., Uchida, S., and Sasaki, S. (2010) *J. Biol. Chem.* **285,** 40777–40784
6. Wan, X., Steudle, E., and Hartung, W. (2004) *J. Exp. Bot.* **55,** 411–422
7. Hub, J. S., Aponte-Santamaria, C., Grubmüller, H., and de Groot, B. L. (2010) *Biophys. J.* **99,** L97–L99

8. Lorenz, D., Krylov, A., Hahm, D., Hagen, V., Rosenthal, W., Pohl, P., and Maric, K. (2003) *EMBO Rep.* **4,** 88–93
9. Stefan, E., Wiesner, B., Baillie, G. S., Mollajew, R., Henn, V., Lorenz, D., Furkert, J., Santamaria, K., Nedvetsky, P., Hundsrucker, C., Beyermann, M., Krause, E., Pohl, P., Gall, I., MacIntyre, A. N., Bachmann, S., Houslay, M. D., Rosenthal, W., and Klussmann, E. (2007) *J. Am. Soc. Nephrol.* **18,** 199–212
10. Zampighi, G. A., Kreman, M., Boorer, K. J., Loo, D. D., Bezanilla, F., Chandy, G., Hall, J. E., and Wright, E. M. (1995) *J. Membr. Biol.* **148,** 65–78
11. Hoffert, J. D., Pisitkun, T., Wang, G., Shen, R. F., and Knepper, M. A. (2006) *Proc. Natl. Acad. Sci. U.S.A.* **103,** 7159–7164
12. Strange, K., and Spring, K. R. (1987) *Science* **235,** 1068–1070
13. Matsui, H., Davis, C. W., Tarran, R., and Boucher, R. C. (2000) *J. Clin. Invest.* **105,** 1419–1427
14. Pohl, P., Saparov, S. M., Borgnia, M. J., and Agre, P. (2001) *Proc. Natl. Acad. Sci. U.S.A.* **98,** 9624–9629
15. Mollajew, R., Zocher, F., Horner, A., Wiesner, B., Klussmann, E., and Pohl, P. (2010) *Biophys. J.* **99,** 3647–3656
16. Magde, D., Elson, E., and Webb, W. W. (1972) *Phys. Rev. Lett.* **29,** 705–708
17. Magde, D., Elson, E. L., and Webb, W. W. (1974) *Biopolymers* **13,** 29–61
18. Gendron, P. O., Avaltroni, F., and Wilkinson, K. J. (2008) *J. Fluoresc.* **18,** 1093–1101
19. Schwille, P., Korlach, J., and Webb, W. W. (1999) *Cytometry* **36,** 176–182
20. Petrásek, Z., and Schwille, P. (2008) *Biophys. J.* **94,** 1437–1448
21. Kovbasnjuk, O., Leader, J. P., Weinstein, A. M., and Spring, K. R. (1998) *Proc. Natl. Acad. Sci. U.S.A.* **95,** 6526–6530
22. von Bonsdorff, C. H., Fuller, S. D., and Simons, K. (1985) *EMBO J.* **4,** 2781–2792
23. van Meer, G., and Simons, K. (1986) *EMBO J.* **5,** 1455–1464
24. Simons, K., and van Meer, G. (1988) *Biochemistry* **27,** 6197–6202
25. Maric, K., Wiesner, B., Lorenz, D., Klussmann, E., Betz, T., and Rosenthal, W. (2001) *Biophys. J.* **80,** 1783–1790
26. Tsunoda, S. P., Wiesner, B., Lorenz, D., Rosenthal, W., and Pohl, P. (2004) *J. Biol. Chem.* **279,** 11364–11367
27. Missner, A., Kügler, P., Saparov, S. M., Sommer, K., Mathai, J. C., Zeidel, M. L., and Pohl, P. (2008) *J. Biol. Chem.* **283,** 25340–25347
28. Yang, B., and Verkman, A. S. (1997) *J. Biol. Chem.* **272,** 16140–16146
29. van Hoek, A. N., and Verkman, A. S. (1992) *J. Biol. Chem.* **267,** 18267–18269
30. Zeidel, M. L., Ambudkar, S. V., Smith, B. L., and Agre, P. (1992) *Biochemistry* **31,** 7436–7440
31. Chou, C. L., Yu, M. J., Kassai, E. M., Morris, R. G., Hoffert, J. D., Wall, S. M., and Knepper, M. A. (2008) *Am. J. Physiol. Renal Physiol.* **295,** F192–F201
32. Heo, J., Meng, F., and Hua, S. Z. (2008) *Anal. Chem.* **80,** 6974–6980